

## THE EVOLUTION IN THE FAINT-END SLOPE OF THE QUASAR LUMINOSITY FUNCTION

PHILIP F. HOPKINS<sup>1</sup>, LARS HERNQUIST<sup>1</sup>, THOMAS J. COX<sup>1</sup>, BRANT ROBERTSON<sup>1</sup>, TIZIANA DI MATTEO<sup>2</sup>, & VOLKER SPRINGEL<sup>3</sup>

Submitted to *ApJ*, August 5, 2005

### ABSTRACT

Based on numerical simulations of galaxy mergers that incorporate black hole growth, we predict the faint end slope of the quasar luminosity function (QLF) and its evolution with redshift. Our simulations have yielded a new model for quasar lifetimes and light curves where the lifetime depends on both the instantaneous *and* peak luminosities of the quasar. This description motivates a new interpretation of the quasar luminosity function in which the bright end of the QLF consists of quasars radiating near their peak luminosities, but the faint end is mostly made up of brighter peak luminosity quasars seen in less luminous phases of evolution. The faint-end QLF slope is then determined by the faint-end slope of the quasar lifetime for quasars with peak luminosities near the observed break. We determine this slope from the quasar lifetime as a function of peak luminosity, based on a large set of simulations which encompass a wide variety of host galaxy, merger, black hole, and interstellar gas properties. Brighter peak luminosity (higher black hole mass) systems undergo more violent evolution, and expel and heat gas more rapidly in the final stages of quasar evolution, resulting in a flatter faint-end slope (as these objects fall below the observed break in the QLF more rapidly). Therefore, as the QLF break luminosity moves to higher luminosities with increasing redshift, implying a larger typical quasar peak luminosity, the faint-end QLF slope flattens. From our determined quasar lifetimes as a function of peak luminosity and this interpretation of the QLF, we predict the faint-end QLF slope and its evolution with redshift in good agreement with observations. Although black holes grow in an anti-hierarchical manner (with lower-mass black holes formed primarily at lower redshifts), the observed change in slope and differential or “luminosity dependent density evolution” in the QLF is completely determined by the non-trivial, luminosity-dependent quasar lifetime and physics of quasar feedback, and not by changes in the shape of the underlying peak luminosity or active black hole mass distributions.

*Subject headings:* quasars: general — galaxies: active — galaxies: evolution — cosmology: theory

### 1. INTRODUCTION

The shape and evolution of the quasar luminosity function (QLF) is fundamental to cosmology, constraining theories of galaxy and supermassive black hole (BH) formation, accretion models, the X-ray, UV, and infrared backgrounds, the role of galaxy mergers and interactions, and reionization. Until recently, it has not been possible to reliably measure the faint-end slope of the QLF even at low redshifts, but this has begun to change with the advent of large, uniformly selected quasar samples in surveys such as the SDSS and 2dF which now increasingly probe the QLF to fainter luminosities. Furthermore, a growing number of observations at different redshifts, in radio, optical, and soft and hard X-ray bands, have suggested that the faint end slope evolves, becoming flatter at higher redshift (e.g. Page et al. 1997; Miyaji et al. 2000, 2001; La Franca et al. 2002; Cowie et al. 2003; Ueda et al. 2003; Fiore et al. 2003; Hunt et al. 2004; Cirasuolo et al. 2005; Hasinger et al. 2005).

This evolution, parameterized either as direct evolution in the faint-end slope or as “luminosity-dependent density evolution” (LDDE), has been the subject of much speculation, as it implies that the density of lower-luminosity quasars peaks at lower redshift. In traditional models of the quasar lifetime and light curve, this evolution must be directly related to the distribution of quasar hosts, implying e.g. significant

and rapid evolution in the *shape* of the distribution of host galaxy masses, which cannot be accounted for in either semi-analytical models or numerical simulations and is not consistent with a wide range of galaxy observations. Although models which adopt these simplified prescriptions for quasar evolution have had success predicting the evolution of the *bright* end of the QLF (e.g. Kauffmann & Haehnelt 2000; Wyithe & Loeb 2003), they do not predict the faint-end slope or its evolution, and as such cannot be reliably extrapolated to low luminosities or to redshifts where the slope is undetermined. Observations of the high-redshift, faint end quasar luminosity function slope are highly uncertain, and no large, uniformly selected samples yet exist which measure the faint-end slope at both low ( $z \lesssim 1$ ) and high ( $z \gtrsim 3$ ) redshifts, and therefore theoretical models of the faint-end slope are especially important. This high- $z$ , faint-end slope is a critical quantity in determining the early formation history of black holes and, especially, their contribution to reionization, as well as possible connections between quasars and e.g. the low-luminosity Seyferts seen at  $z \sim 0$ .

Without a more sophisticated model of quasar evolution, models which have attempted to reconcile observations of evolution in the faint-end QLF slope and BH populations (e.g., Merloni 2004) have been forced to fit to the entire QLF and BH mass distribution to essentially arbitrary distributions of lifetimes/duty cycles and accretion rates as a function of redshift. Still, this phenomenological modeling has elucidated the anti-hierarchical nature of BH growth, with smaller-mass BHs formed at lower redshift as an implication of this evolution in the QLF. But an actual prediction of the faint-end slope requires a more detailed model for both quasar lifetimes and the QLF.

<sup>1</sup> Harvard-Smithsonian Center for Astrophysics, 60 Garden Street, Cambridge, MA 02138, USA

<sup>2</sup> Carnegie Mellon University, Department of Physics, 5000 Forbes Ave., Pittsburgh, PA 15213

<sup>3</sup> Max-Planck-Institut für Astrophysik, Karl-Schwarzschild-Straße 1, 85740 Garching bei München, Germany

Recently, BH growth and feedback have been incorporated into numerical simulations of galaxy mergers (Springel et al. 2005a,b, Springel 2005, Di Matteo et al. 2005). In these simulations, gravitational torques drive inflows of gas into the nuclei of merging galaxies (e.g. Barnes & Hernquist 1991, 1996), triggering starbursts (e.g. Mihos & Hernquist 1996) and feeding the growth of central supermassive BHs (Di Matteo et al. 2005). As the BHs accrete, some of the radiated energy couples to the surrounding gas, and the growth eventually stalls when this feedback energy is sufficient to unbind the reservoir of gas. These simulations elucidate the connection between galaxy evolution, the formation of supermassive BHs, and the self-regulated nature of quasar activity, and provide quantitative predictions which agree well with observations of, e.g., the  $M_{\text{BH}} - \sigma$  relation (Di Matteo et al. 2005, Robertson et al. 2005), quasar lifetimes (Hopkins et al. 2005a,b), and the QLF in various wavebands (Hopkins et al. 2005c,d,e). These simulations provide a fully self-consistent, quantitative prediction of the light curve of quasar activity and the resulting quasar “lifetime” – i.e., the amount of time that a quasar spends at a given luminosity – and its dependence on the properties of the merging galaxies.

The resulting quasar light curves imply a qualitatively different picture of the QLF than previously considered (Hopkins et al. 2005c). Specifically, in the model of Hopkins et al. (2005a-f), quasars evolve rapidly and their lifetime depends on both their instantaneous *and* peak luminosities. Critically, the quasar lifetime in this model is longer at lower luminosities; i.e. a given quasar spends more time (and is more likely to be observed) at a luminosity well below its peak luminosity. This differs from previous models which generally assume that quasars radiate at a fixed luminosity for some characteristic lifetime, or adopt simplified exponential light curves. In our picture, the bright end of the QLF consists of quasars growing rapidly and radiating near their peak luminosities, while the faint end consists of quasars either undergoing exponential growth to much larger masses and higher luminosities, or in sub-Eddington quiescent states going into or coming out of a period of peak activity. The “break” in the QLF corresponds directly to the maximum in the intrinsic distribution of *peak* luminosities, which falls off at both brighter and fainter luminosities. The faint-end QLF slope is then determined by the faint-end slope of the luminosity-dependent quasar lifetime (i.e. the differential time the quasar spends in any given luminosity interval), for quasars with peak luminosity near the observed break. In other words, the number of quasars in efficient, near-peak growth stages needed to account for the observed bright end of the QLF is already sufficient to account for the observed faint end, as any given quasar is much more likely to be observed at luminosities well below its peak, and thus the probability of seeing such brighter sources at these lower luminosities entirely determines the shape of the faint-end QLF.

This modeling of the quasar lifetime, and the corresponding interpretation of the QLF, then provides a physical motivation for the location of the break luminosity and the faint-end slope of the observed QLF (Hopkins et al. 2005c,d,e). Furthermore, Hopkins et al. (2005e) demonstrate that this description accurately predicts a large number of quasar observations, including the QLF in all wavebands and at all redshifts, the distribution of Eddington ratios as a function of luminosity and redshift, the BH mass function (both of active and relic BHs), the distribution of column densities and obscured fraction as a function of luminosity, the X-ray background spectrum, and

the anti-hierarchical BH growth described above. Given this remarkable agreement and the simple physical motivation for the faint-end QLF slope unique to this modeling, it should account for both the value and evolution of this slope with redshift.

In this paper, we use our picture of quasar lifetimes and the resulting QLF interpretation from Hopkins et al. (2005a-f) to predict the faint-end slope of the quasar lifetime as a function of quasar peak luminosity, which in this model can be immediately translated to a prediction of the faint-end QLF slope as a function of the QLF break luminosity and, consequently, as a function of redshift. We are able to accurately predict the observed evolution in the slope and corresponding LDDE based only on the input physics of our hydrodynamic simulations, as a unique consequence of our interpretation of the QLF and without the need to invoke any evolution in the shape of e.g. the quasar host or galaxy mass distribution. We further develop a simple analytical model of quasar feedback which gives similar predictions, and demonstrates the scale-dependent feedback physics which drive the evolution of the faint-end slope.

Throughout, we define  $L = L_{\text{bol}}$ , the bolometric luminosity. We denote the faint-end slope  $\gamma$  by  $\phi = d\Phi/d\log(L) \propto L^{-\gamma}$ , where  $\phi$  is the differential *bolometric* QLF and we are considering luminosities  $L \ll L_*$ , where  $L_*$  is the “break” in the QLF. Note that  $d\Phi/dL \propto L^{-\gamma-1}$ , as e.g. in the standard “double power law” form of the QLF. The sign convention (i.e. *positive*  $\gamma$ ) also follows the general observational convention and standard double power law convention, with  $d\Phi/dL \propto 1/\{(L/L_0)^{\gamma_1+1} + (L/L_0)^{\gamma_2+1}\}$ . We adopt a  $\Omega_M = 0.3$ ,  $\Omega_\Lambda = 0.7$ ,  $H_0 = 70 \text{ km s}^{-1} \text{ Mpc}^{-1}$  cosmology.

## 2. THE FAINT-END SLOPE AS A FUNCTION OF PEAK LUMINOSITY

If quasars spend a differential time  $dt_Q/d\log(L)$  per logarithmic interval in luminosity, then the observed QLF is (at times when the quasar lifetime is short compared to the Hubble time)

$$\phi(L) = \int dt_Q/d\log(L) \dot{n}(L_{\text{peak}}) d\log L_{\text{peak}}, \quad (1)$$

where  $\dot{n}(L_{\text{peak}})$  is the rate at which quasars of a given peak luminosity  $L_{\text{peak}}$  are created or activated (per unit time per unit comoving volume per logarithmic interval in  $L_{\text{peak}}$ ). In Hopkins et al. (2005c,e), we use this and the realistic modeling of quasar lifetimes from Hopkins et al. (2005a,b,e) to determine  $\dot{n}(L_{\text{peak}})$ , and find that it does *not* have the same shape as the observed QLF, as is predicted by simple models in which the quasar turns “on/off” as a step function or follows a pure exponential light curve. Instead,  $\dot{n}(L_{\text{peak}})$  traces the shape of the observed QLF at the bright end (above  $L_*$ ), peaks at  $L_{\text{peak}} \sim L_*$ , then falls off below this. Therefore, the slope of the faint-end QLF,  $\gamma$ , is dominated by the faint-end slope of  $dt_Q/d\log(L)$  for quasars with  $L_{\text{peak}} \sim L_*$ ; i.e. the observed faint end of the QLF is dominated by brighter *peak* luminosity sources, accreting efficiently but in early merger stages or in sub-Eddington states transitioning into or out of peak quasar activity, so  $\gamma$  is determined by the integrated probability of seeing the population of brighter  $L_{\text{peak}}$  sources, dominated by sources with  $L_{\text{peak}} \sim L_*$ , at lower  $L$ .

Given this interpretation of the QLF,  $\gamma$  should be simply calculable from the  $L \ll L_{\text{peak}}$  slope of  $dt_Q/d\log(L)$  (since the probability of seeing such a source at  $L$  is proportional to its lifetime at  $L$ ), for sources with  $L_{\text{peak}} \approx L_*$ . If the quasar lifetime is a function of  $L$  and  $L_{\text{peak}}$  only (i.e. not affected

systematically by other host galaxy properties), then  $\gamma$  can be entirely predicted by knowing  $L_*(z)$ , which directly gives the peak in the  $\dot{n}(L_{\text{peak}})$  distribution as a function of redshift. There may be some curvature introduced because of the non-zero contributions to the faint-end of the QLF from sources with  $L_{\text{peak}} \neq L_*$ , but as such corrections depend on the exact shape of  $\dot{n}(L_{\text{peak}})$  and are small, as  $\dot{n}(L_{\text{peak}})$  drops off rapidly (as the bright-end QLF does) away from  $L = L_*$ , we ignore them here.

### 2.1. The Quasar Lifetime from Simulations

We first consider the  $L \ll L_{\text{peak}}$  behavior of the quasar lifetime determined from hydrodynamical simulations. We consider a suite of several hundred simulations, described in detail in Robertson et al. (2005) and Hopkins et al. (2005e). These were performed with the new parallel TreeSPH code GADGET-2 (Springel 2005), which uses an entropy-conserving formulation of smoothed particle hydrodynamics (SPH; Springel & Hernquist 2002), and includes a sub-resolution, multiphase model of the dense interstellar medium (ISM) to describe star formation (Springel & Hernquist 2003). The multiphase gas is pressurized by feedback from supernovae, allowing us to stably evolve even pure gas disks (see, e.g. Springel et al. 2005b, Robertson et al. 2004, Springel & Hernquist 2005). BHs are represented by “sink” particles that accrete gas, with an accretion rate  $\dot{M}$  estimated using a Bondi-Hoyle-Lyttleton parameterization, with an upper limit equal to the Eddington rate (Springel et al. 2005b). The bolometric luminosity of the BH is then  $L = \epsilon_* \dot{M} c^2$ , where  $\epsilon_* = 0.1$  is the radiative efficiency. We further allow a small fraction (typically  $\approx 5\%$ ) of  $L$  to couple dynamically to the gas as thermal energy. This fraction is a free parameter, determined in Di Matteo et al. (2005) by fitting the  $M_{\text{BH}}-\sigma$  relation. We generate two stable, isolated disk galaxies, each with an extended dark matter halo having a Hernquist (1990) profile, an exponential disk, and a bulge. The galaxies are then set to collide from a zero energy orbit.

In our suite of simulations, we vary the masses and virial velocities of the initial galaxies, halo concentrations, ISM equation of state, parameters describing feedback from supernovae and black hole growth, presence or absence of bulges in the host galaxies, initial BH seed masses, numerical resolution (typically  $\sim 2 \times 10^5$  particles per galaxy, but we consider up to 10-100 times as many), disk inclinations and pericenter separation of the initial orbits, and initial disk gas fractions. We further scale all galaxy properties appropriately to resemble galaxies at redshifts  $z = 0-6$ , for a large subset of our simulations as described in Robertson et al. (2005). Our simulations produce quasars with  $L$ ,  $L_{\text{peak}}$  from  $\sim 10^8 - 10^{15} L_{\odot}$ , spanning the entire range of observed quasar luminosities at all redshifts. Hopkins et al. (2005e) consider this set of simulations in detail, and use it to determine the quasar lifetime  $dt_Q/d\log(L)$ . Critically, they find that  $dt_Q/d\log(L)$  shows *no* systematic dependence and little scatter with any of the varied parameters, when quantified as a function of  $L$  and  $L_{\text{peak}}$ . The predictions in Hopkins et al. (2005e) did not depend sensitively on the (much more uncertain) faint-end slope, and therefore the authors did not consider a detailed fit to the faint-end behavior of  $dt_Q/d\log(L)$ , but rather parameterized the lifetime as a simple exponential,  $dt_Q/d\log(L) = t_0 \exp(-L/L_0)$ , where  $L_0 \approx 0.2L_{\text{peak}}$  and  $t_0$  depends weakly on  $L_{\text{peak}}$ , which provides an excellent fit to the simulation results for  $L \gtrsim 10^{-2} - 10^{-1} L_{\text{peak}}$ . Hopkins et al. (2005b) consider the

$L \ll L_{\text{peak}}$  behavior of  $dt_Q/d\log(L)$  in more detail, and find that the lifetime more closely resembles a power law at these  $L$ , with a power-law slope  $\alpha$  a function of  $L_{\text{peak}}$ . The combination of these results suggests that the quasar lifetime is best parameterized as a Schechter function with slope  $\alpha$ , normalization  $t_0(L_{\text{peak}})$ , and turnover  $L_0(L_{\text{peak}})$ , for purposes where the faint-end slope is important; i.e. (to clarify our conventions)

$$\frac{dt_Q}{d\log(L)} = t_0 \left(\frac{L}{L_0}\right)^{-\alpha} \exp\left(-\frac{L}{L_0}\right). \quad (2)$$

For a QLF with break  $L_*(z)$ , which implies an  $\dot{n}(L_{\text{peak}})$  distribution peaked at  $L_{\text{peak}} \sim L_*$ , the observed faint-end QLF slope is then  $\gamma \approx \alpha(L_{\text{peak}} = L_*)$ .

Here, we consider the faint-end ( $L \ll L_{\text{peak}}$ ) slope from these simulations in greater detail. For each simulation, we fit a Schechter function to the quasar lifetime as a function of luminosity. We find similar results to Hopkins et al. (2005e) for  $L_0$  and  $t_0$  (allowing for the well-known degeneracy between  $t_0$  and  $\alpha$  in these fits), but now quantify  $\alpha$  as a function of  $L_{\text{peak}}$ . As discussed in Hopkins et al. (2005c,e), these faint-end slopes are subject to several uncertainties in our modeling (the reason for ignoring the correction at very low luminosities implied by  $\alpha$  in Hopkins et al. 2005e). One is the finite time duration of our simulations, which may flatten  $dt_Q/d\log(L)$  at low  $L$ , as the BH cannot completely relax in the given time. A complementary means to determine  $\gamma$  is then to consider the rate at which  $L$  falls off after  $L = L_{\text{peak}}$  at time  $t = t_p = t(L_{\text{peak}})$ . We take  $L(t)/L_{\text{peak}}$  to be a function of  $t - t_p$ , and find that it falls off in approximate power-law fashion for all our simulations,  $L(t) \propto (t - t_p)^{-\beta}$ . This implies  $dt_Q/d\log(L) \propto L^{-1/\beta}$ , i.e.  $\gamma = \alpha = 1/\beta$ . Although these fits are not affected by the finite time duration of the simulations, they do not include the time spent at different  $L$  before  $L = L_{\text{peak}}$ , and thus are entirely accurate only at  $t \gg t_p$  or for a symmetric rise/fall in  $L$ , and may therefore overestimate the steepness of  $\gamma$ , so we consider both fitting methods below.

The uncertainties in this modeling at low luminosities are discussed in detail by Hopkins et al. (2005c,e). Hopkins et al. (2005b) examine fits to the power-law behavior of  $dt_Q/d\log(L)$  at  $L \ll L_{\text{peak}}$  considering both the entire simulation and only times after the merger (similar to our fits for the decay of  $L(t)$ ). Further, Hopkins et al. (2005c) consider the application of an ADAF-type correction for radiatively inefficient accretion flows at low accretion rates (following e.g., Narayan & Yi 1995), to account for more detailed variation in the radiative efficiency and spectrum as a function of accretion rate. We apply this correction in our fitting as well. Although these previous works consider a much smaller subset of the simulations we have fit to, they find similar results, and we compare their fits and ours below to demonstrate both the general agreement and range of uncertainty introduced by these different determinations of  $\gamma$ .

Figure 1 shows the results of this fitting for several representative simulations. We show the lifetime as a function of  $L$  (for clarity, the integrated lifetime above a given  $L$ ,  $t_Q(L' > L)$ , is shown), for simulations with  $L_{\text{peak}}/L_{\odot} = 3.1 \times 10^{12}$  (black circles),  $7.3 \times 10^{12}$  (blue diamonds),  $1.7 \times 10^{13}$  (green squares),  $1.4 \times 10^{14}$  (red  $\times$ 's), and the best-fit Schechter function (solid lines) to each, with slope  $\alpha$ , on the left. We compare these to the slopes  $1/\beta$  determined by fitting  $L(t)/L_{\text{peak}}$  as a function of  $t - t_p$  (right, same notation). The resulting faint-end slope  $\gamma$  for each  $L_{\text{peak}}$  and each fitting method are also shown; there is a clear decrease of  $\gamma$  with

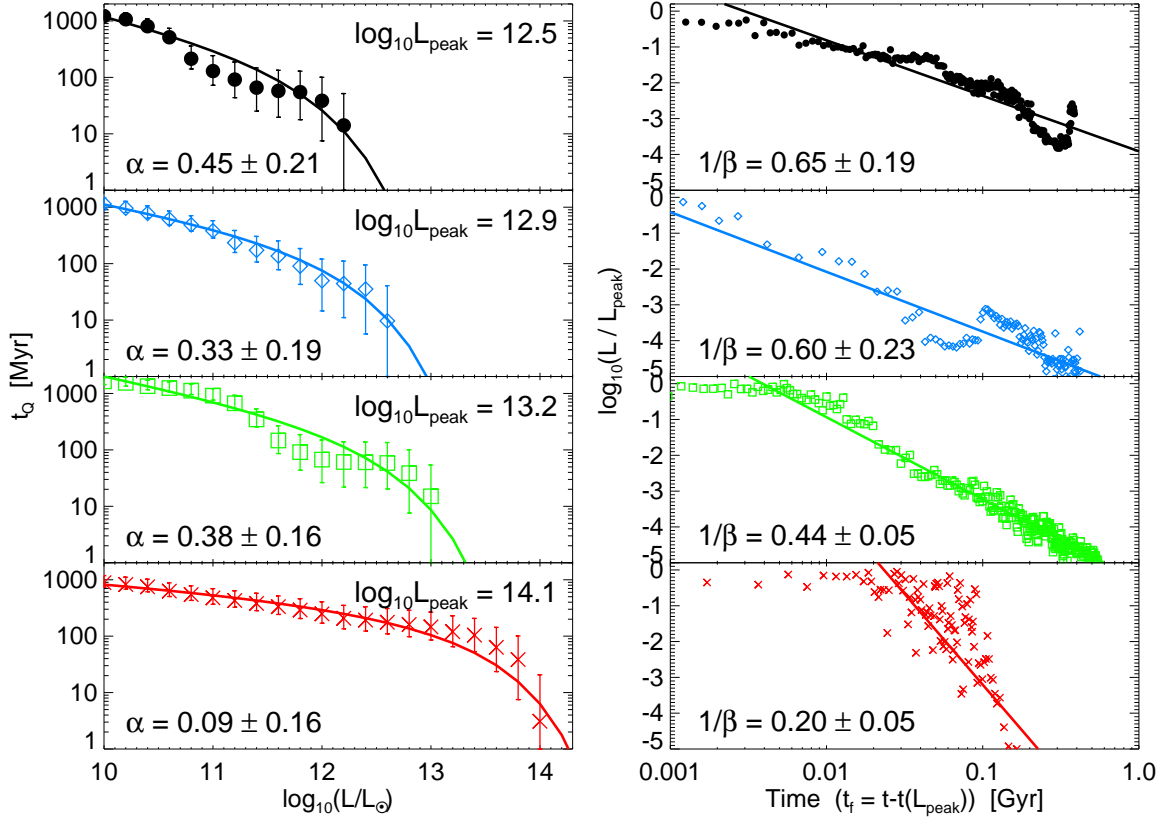


FIG. 1.— Left: Quasar lifetime (integrated time above a given  $L$ ), for representative mergers with peak luminosities  $L_{\text{peak}}/L_{\odot} = 3.1 \times 10^{12}$  (black circles),  $7.3 \times 10^{12}$  (blue diamonds),  $1.7 \times 10^{13}$  (green squares),  $1.4 \times 10^{14}$  (red  $\times$ 's), with the best-fit Schechter functions (lines) of slope  $\alpha$ . Right: Bolometric luminosity over peak luminosity ( $L/L_{\text{peak}}$ ) as a function of time ( $t_f = t - t(L_{\text{peak}})$ ), with the best-fit power law of slope  $\beta$ . The predicted faint-end LF slopes  $\gamma = \alpha = 1/\beta$  are also shown.

TABLE 1  
FAINT-END SLOPE  $\gamma(L_{\text{peak}})$

Determination <sup>a</sup>	$\gamma_{12} = \gamma(L_{\text{peak}} = 10^{12} L_{\odot})$	$\frac{d\gamma}{d \log(L_{\text{peak}})}$
H05b, all times	$0.95 \pm 0.25$	$-0.32 \pm 0.11$
H05b, $t \gtrsim t(L_{\text{peak}})$	$0.76 \pm 0.20$	$-0.30 \pm 0.07$
H05c, all times	$0.94 \pm 0.20$	$-0.33 \pm 0.08$
H05c, $t \gtrsim t(L_{\text{peak}})$	$0.50 \pm 0.15$	$-0.50 \pm 0.15$
Schechter fitting	$0.44 \pm 0.02$	$-0.21 \pm 0.02$
$L(t) \propto t^{\beta}$ decay	$0.69 \pm 0.05$	$-0.30 \pm 0.04$
Cumulative best-fit	$0.55 \pm 0.12$	$-0.25 \pm 0.04$
Blastwave model	$0.35 \pm 0.15$	$-0.22 \pm 0.06$

<sup>a</sup>H05b, H05c (Hopkins et al. 2005b,c) use a small subset of the simulations here, with H05c applying an ADAF-type correction at low accretion rates.

$L_{\text{peak}}$ .

We fit for  $\gamma(L_{\text{peak}})$  in each of our suite of several hundred simulations with both methods described above. In all cases we find  $\gamma$  decreases with  $L_{\text{peak}}$  in a manner similar to that in Figure 1. Given the scatter, the resulting slopes  $\gamma(L_{\text{peak}})$  are well fitted by a simple log-linear relation,

$$\gamma(L_{\text{peak}}) = \gamma_{12} + \frac{d\gamma}{d \log(L_{\text{peak}})} (\log(L_{\text{peak}}/L_{\odot}) - 12), \quad (3)$$

where  $\gamma_{12} \sim 0.5$  and  $\frac{d\gamma}{d \log(L_{\text{peak}})} \sim -0.3$ . This is illustrated in Figure 2, where the value of  $\gamma$  determined from fitting Schechter functions to the quasar lifetime for each of our sim-

ulations is plotted as a function of the peak luminosity of those simulations (circles, with errors), with the best-fit log-linear relation (line) (see also Figure 7 of Hopkins et al. 2005b). The results for both fitting methods are summarized in Table 1. We also show the results of Hopkins et al. (2005b,c), described previously. As shown in detail in Hopkins et al. (2005e), we find no systematic dependence on redshift, host galaxy properties, or any other varied parameters in the simulations.

In our simulations, gas is expelled when feedback from accretion heats the surrounding gas to the point where it can no longer efficiently cool and rapidly unbinds it. Around more massive BHs (i.e. higher- $L_{\text{peak}}$  quasars), this “blowout” event is progressively more violent; the higher luminosity of the quasar heats the gas more rapidly and to higher temperatures, resulting in a more violent and complete expulsion of gas (see also Cox et al. 2005, who show the gas mass fraction expelled increases with BH mass). This is clear in the representative simulations for which we fit  $L(t - t_p)$ , which falls off much more rapidly in higher- $L_{\text{peak}}$  simulations as the density decreases and temperature (sound speed) increase more dramatically around the quasar.

## 2.2. A Simple Model of Quasar Feedback

To understand this trend in greater detail, we consider an analytical model for the quasar “blowout” event, i.e. the rapid heating and expulsion of gas when the quasar reaches a critical mass/luminosity, in agreement with the  $M_{\text{BH}} - \sigma$  relation. We can use such a model to predict and understand at least the late-time (post critical mass) evolution of the quasar accretion

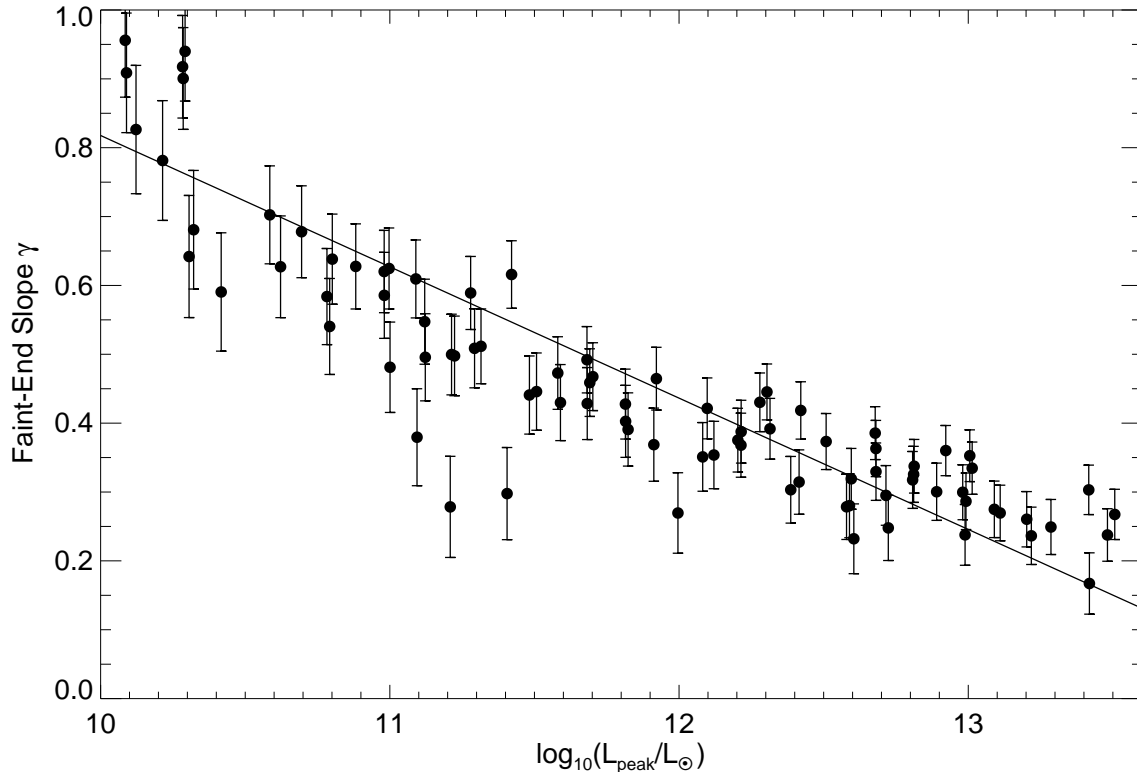


FIG. 2.— Faint-end QLF/quasar lifetime slope  $\gamma = \alpha$  determined from fits to the quasar lifetime as a function of peak luminosity  $L_{\text{peak}}$  in our simulations. The best-fit log-linear relation (see Table 1) is shown (solid line).

rate, although the early activity (which as demonstrated above is a significant contributor to the lifetime at low- $L$ ) is determined by the chaotic merger process and is much more difficult to accurately predict in simple analytical form. We note that this problem has been considered in greater detail in previous works (e.g. Barkana & Loeb 2001; Furlanetto & Loeb 2001; Scannapieco & Oh 2004), but these authors have considered the large-scale structure and impact of these outflows on the outer regions of halos and clusters, the surrounding IGM, and reionization; we are instead interested in the very small scale, rapid expulsion of gas from the innermost BH-dominated accretion regions of the galaxy. Interestingly, these works suggest that feedback on these scales is critical in regulating the slope of the *bright* end of the QLF, which highlights the importance of quasar feedback on all scales in the QLF.

In our numerical modeling (Di Matteo et al. 2005) and most analytical models of the  $M_{\text{BH}} - \sigma$  relation (e.g., Silk & Rees 1998; Fabian 1999; Ciotti & Ostriker 2001; Wyithe & Loeb 2002), feedback energy from accretion onto the central BH heats the surrounding gas (or momentum from coupling of the radiation field to dust drives a wind). In earlier stages of BH growth, this is a small luminosity, and the gas is able to efficiently cool and re-radiate this energy. However, in the peak merger stages, the BH growth is exponential (Eddington-limited), and as it rapidly grows in luminosity, a critical threshold is reached where the nearby gas can no longer cool efficiently in a local dynamical time. As a result, the gas is rapidly expelled, and what remains is heated to virial temperatures, preventing it from being easily accreted, and further accretion shuts down. The threshold for this behavior is deter-

mined by the local gas properties and gravitational potential of the host, but essentially all models of feedback driven self-regulation (owing to exceeding a critical energy input in of order a dynamical time) predict a relation between final black hole mass and virial velocity or spheroid velocity dispersion of roughly  $M_{\text{BH}} \propto V_{\text{vir}}^5$  or  $M_{\text{BH}} \propto \sigma^4$ , respectively.

Because the gas in the central galaxy regions is able to efficiently cool prior to this self-regulation, and is then suddenly heated and driven out in a short time (in our simulations, this occurs over a timescale  $\sim 10^7$  yr in massive mergers) by an exponentially increasing luminosity, it is reasonable to model this driven outflow phase as a Sedov-Taylor-type blastwave (Sedov 1946, 1959; Taylor 1950), with energy injection from a point explosion with energy  $E = \eta_L L_{\text{Edd}}(M_{\text{BH}}^f) t_{\text{dyn}}$  ( $\eta_L$  describes the efficiency of feedback coupling,  $\approx 5\%$  in our simulations and similar in most analytical models of the  $M_{\text{BH}} - \sigma$  relation). A more detailed examination of this problem in e.g. Furlanetto & Loeb (2001) shows that this is a remarkably accurate approximation to a full solution including radiative cooling, the pressure of the external medium, magnetic fields, and further effects. Modeling the accretion rate with a Bondi-Hoyle (Bondi & Hoyle 1944; Bondi 1952) parameterization (as by definition we are considering times when the accretion rate falls below the Eddington limit), considered at the radius of influence of the BH,  $R_{\text{BH}} = GM_{\text{BH}}\sigma^{-2}$  ( $\sigma$  being the spheroid velocity dispersion) gives  $L \propto M_{\text{BH}}^2 \rho(R_{\text{BH}}) c_s^{-3}(R_{\text{BH}})$ , where  $c_s$  is the isothermal sound speed (in our simulations, the effective sound speed of the multi-phase ISM is used, see Springel & Hernquist 2003). As the accretion rate is rapidly falling from its peak during this stage, we can reasonably approxi-

mate  $M_{\text{BH}} = M_{\text{BH}}^f = \text{constant}$ , and thus  $R_{\text{BH}} = \text{constant}$ , and we only need to calculate the time evolution of the gas density  $\rho$  and sound speed  $c_s$  at fixed  $r = R_{\text{BH}}$  to determine the time evolution of luminosity  $L$  in this stage. We are only interested in the scaling of  $L(t) \propto t^{-\beta}$  (where  $t$  here is the time since the peak quasar luminosity or beginning of this “blowout” stage), so we could theoretically pick any fixed radius to evaluate these quantities, and thus the choice of the radius of influence of the BH as opposed to the transonic radius, for example, is not significant.

We first consider the simplest, scale-invariant solution to this problem, in which we neglect the gravitational field of the BH and halo, following Ostriker & McKee (1988) in our derivation. We also ignore the consequences of radiation as noted above, but this should not be a large effect in the very inner regions of the blastwave expansion in which we are interested (see also Murray et al. 2005, who consider in detail the coupling of BH radiation to dust and gas opacity and show that it produces a very similar  $M_{\text{BH}} - \sigma$  relation and qualitative “blowout” behavior). As we need to describe  $\rho(r, t)$  at small radii (relative to the galaxy size and final radius of the blastwave), we must consider the density gradient of the medium, for which we adopt the one-power approximation (OPA)  $\rho \propto r^{-k_\rho}$  for the ambient (pre-shocked) medium. There may be some non-spherical effects due to asymmetry in the density profile or e.g. bipolar outflows driven by the quasar, but the result is qualitatively quite similar to the spherical solution along any given sightline, and we furthermore expect that the chaotic interactions and short dynamical times in the central regions of the merger will rapidly isotropise the region of interest. For a self-similar OPA Sedov-Taylor solution, the shock radius  $R_s$  expands as  $R_s \propto t^\eta$  with the post-shock (internal) density profile  $\rho = \rho_1 (r/R_s)^{l_\rho}$ , where  $\rho_1 \propto \rho(R_s)$  is the density just inside the shock front. At fixed  $r = R_{\text{BH}}$ , then, we have

$$\rho(R_{\text{BH}}, t) \propto t^{-(k_\rho + l_\rho)\eta}. \quad (4)$$

For a self-similar, energy-conserving blastwave,  $\eta = 2/(5 - k_\rho)$ , and mass conservation (coupled with the strong shock jump conditions;) requires  $l_\rho = (6 - (\gamma_{\text{EOS}} + 1)k_\rho)/(\gamma_{\text{EOS}} - 1)$ . Here, we denote the ratio of specific heats as  $\gamma_{\text{EOS}}$  to distinguish it from the faint-end QLF slope  $\gamma$ . We then obtain

$$(k_\rho + l_\rho)\eta = \frac{4}{\gamma_{\text{EOS}} - 1} \left( \frac{3 - k_\rho}{5 - k_\rho} \right). \quad (5)$$

The pressure  $P = \rho c_s^2$  also follows a power-law scaling (with internal power-law slope  $l_p$  and external slope  $k_p$ ), but with a more complicated result for  $l_p$ ,

$$l_p = \frac{3\gamma_{\text{EOS}}^2 + 20\gamma_{\text{EOS}} + 1 - (\gamma_{\text{EOS}} + 1)(3\gamma_{\text{EOS}} + 1)k_\rho}{2(\gamma_{\text{EOS}}^2 - 1)}. \quad (6)$$

Thus the final scaling of  $L(t) \propto \rho c_s^3 \propto \rho^{5/2} P^{-3/2}$  in this phase is given by  $L \propto t^{-\beta}$  with

$$\beta = \frac{10}{\gamma_{\text{EOS}} - 1} \left( \frac{3 - k_\rho}{5 - k_\rho} \right) - 3 \left( \frac{k_p + l_p}{5 - k_\rho} \right). \quad (7)$$

This formalism has an exact, self-consistent solution corresponding to e.g. a blastwave in an isothermal sphere or wind, which should be a reasonable approximation to the mergers our simulations model in detail, with  $k_\rho = 2$  and  $\gamma_{\text{EOS}} = 5/3$  (yielding  $l_\rho = 1$ ,  $l_p = 3$ ). This solution gives  $\beta = 2$ , implying a faint-end QLF slope  $\gamma = 1/2$ . But the above equations should be a good approximation (Ostriker & McKee 1988) for

a range of  $\gamma_{\text{EOS}} \sim 1 - 5/3$  (corresponding to variability in the equation of state owing to the density and temperature dependence of star formation and radiative cooling) and  $k_\rho \sim 1 - 3$  (corresponding to e.g. the inner regions of a Hernquist 1990 spheroid profile with a central point mass). In fact, it is still exact for the equilibrium structure of a filled blastwave with the most natural  $v \propto r$  velocity structure, which yields

$$k_\rho = k_{\rho, \text{crit}} = \frac{7 - \gamma_{\text{EOS}}}{\gamma_{\text{EOS}} + 1}, \quad (8)$$

$$\beta = \frac{1}{3\gamma_{\text{EOS}} - 1} \left[ 20 - \frac{9}{2}(\gamma_{\text{EOS}} + 1) \right]. \quad (9)$$

For the reasonable range of equations of state  $1 \leq \gamma_{\text{EOS}} \leq 5/3$ , this results in  $2 \leq \beta \leq 11/2$ , i.e.  $0.2 \lesssim \gamma \lesssim 0.5$ , in good agreement with the range of  $\gamma$  observed and determined in our simulations.

The scale-invariant Sedov-Taylor solution then explains well the typical values of  $\gamma$  implied by our simulations and the rapid falloff of  $L(t)$  during the “blowout” phase of quasar evolution. However, this does not immediately describe the dependence of  $\gamma$  on  $L_{\text{peak}}$ . This dependence is not contained, as might be presumed from the above derivation, in  $\gamma_{\text{EOS}}$ , as essentially all our simulations have  $\gamma_{\text{EOS}}$  in the entire range  $\sim 1 - 5/3$  in their central regions and we specifically find no significant systematic dependence of  $\gamma$  or the quasar lifetime on the ISM gas equation of state (see also Hopkins et al. 2005e, Figures 4 & 5). Rather, the dependence of  $\gamma$  on  $L_{\text{peak}}$  is driven, naturally, by the fact that this problem is *not* precisely scale invariant or self-similar.

To illustrate the dependence on  $L_{\text{peak}}$ , consider a small change in the initial logarithmic slope of the density in the central regions,  $k_\rho = k_\rho^0 + \delta k_\rho$ . For simplicity we expand about the  $k_\rho^0 = 2$ ,  $\gamma_{\text{EOS}} = 5/3$  exact solution, but our result is similar regardless of the choice of these parameters (within the ranges defined above). This gives

$$\beta = 2 - 13\delta k_\rho/3, \quad (10)$$

$$\gamma = \frac{1}{2} \left( 1 + \frac{13}{6}\delta k_\rho \right), \quad (11)$$

i.e.  $d\gamma/dk_\rho = 13/12$ . Thus, if the initial logarithmic density gradient in the inner regions is *steeper*, i.e. has a larger  $k_\rho$  ( $\rho_0 \propto r^{-k_\rho}$ ), then  $\beta$  is actually *shallower*. In detail, two competing effects occur. First, the density falls off more rapidly, allowing the blastwave front to propagate more rapidly as it builds up more of its mass earlier and encounters less mass further from the central regions, but this effect is relatively weak, i.e.  $\eta \rightarrow \eta + 2\delta k_\rho/9$ . The dominant effect is the alteration of the post-shock density profile. Because the density gradient is steeper, the propagation of the blastwave builds up a less pronounced “snowplow”, i.e. the mass buildup at the wavefront is less pronounced, implying a *flatter* post-shock density gradient by mass conservation (recall that  $\rho$  increases with radius within the shocked region). Essentially, with the gas mass concentrated in the center, the shocked density profile evolves less dramatically, because less mass is added and the early blast is able to effectively redistribute more of the ultimately acquired mass. Given that less massive halos typically have higher concentrations, we can estimate the magnitude of this effect on the evolution of  $\gamma$  with  $L_{\text{peak}}$ . Estimating  $dk_\rho/dc \sim 0.1$  (where  $c$  is the concentration index and we estimate a change  $\sim 10$  in  $c$  changes the inner logarithmic slope at fixed  $r$  by  $\sim 1$ ), we can determine  $dc/d\log(L_{\text{peak}})$

using  $L_{\text{peak}} \propto M_{\text{BH}} \propto M_{\text{vir}}$  (e.g., Marconi & Hunt 2003) and  $c \approx 9(M_{\text{vir}}/10^{13}M_{\odot})^{-0.13}$  (Bullock et al. 2001), and we find

$$\frac{d\gamma}{d\log(L_{\text{peak}})} \sim -0.2 \left( \frac{L_{\text{peak}}}{10^{12}L_{\odot}} \right)^{-0.13}, \quad (12)$$

in reasonable agreement with our measured dependence of  $\gamma(L_{\text{peak}})$  in our simulations and only weakly dependent on  $L_{\text{peak}}$ . This actually predicts that the magnitude of  $d\gamma/d\log L_{\text{peak}}$  should be larger at low- $L_{\text{peak}}$  ( $\sim -0.28$  at  $L_{\text{peak}} \sim 10^{11}L_{\odot}$ ) and smaller at high  $L_{\text{peak}}$ , ( $\sim -0.16$  at  $L_{\text{peak}} \sim 10^{13}L_{\odot}$ ) which may occur (see Figure 2), but this is most likely a coincidence, as our modeling of the blowout in scale invariant fashion and the application of a concentration parameter in such chaotic period in evolution of the merger are rough approximations at best.

In this model of the quasar blowout phase, however, the approximate values for the rate at which accretion declines are simply determined by a standard Sedov-Taylor solution in a medium with a density gradient. The sudden injection of energy as the BH crosses a critical mass/luminosity threshold and the surrounding gas is no longer able to efficiently cool drives a strong outflow and heats the remaining gas, rapidly shutting down accretion. Incorporating the weak, but not negligible, effects of the change in concentration with mass breaks the scale invariance of this solution, as lower-mass systems have steeper inner density profiles, which flatten the evolution of the accretion rate in time and produce steeper  $\gamma$ . Of course, many other effects will break the self-similarity of this problem as well – a realistic gravitational potential will imply a characteristic scale length, and the physics of radiative cooling will likewise define fundamental physical scales. Even the scale-invariant solution incorporating radiative energy loss depends on the logarithmic slope of the cooling function vs. density and temperature, but the values of these slopes depend themselves on the characteristic temperature of the blastwaves and change quite significantly over the mass scale of our simulations (heating to virial temperatures  $c_s^2 \sim \sigma^2$  implies temperatures  $T \sim 10^5 - 10^7$  K over the mass range shown in e.g. Figure 2). Although we do not model the chaotic interactions and evolving BH mass of the early merger stages, the more violent torquing associated with more massive mergers can explain the more rapid, peaked BH evolution over a larger range in BH mass, even in early merger stages, generating a flatter quasar lifetime which spans a wider range in luminosity.

Given these various scalings, it is possible that our observed trend of  $\gamma(L_{\text{peak}})$  could change or even reverse at very low  $L_{\text{peak}}$ , as in models of stellar winds in dwarf ellipticals for which lower-mass objects (lower  $M_{\text{BH}}$ ) are more easily unbound (e.g. Mac Low & Ferrara 1999) (although this is more concerned with the large-scale binding of gas, as opposed to evolution in the inner accretion regions of interest in our modeling), but the masses/luminosities where this is likely to become important ( $M_{\text{gal}} \lesssim 10^8 M_{\odot}$ , i.e.  $L_{\text{peak}} \lesssim 10^9 L_{\odot}$ ) are well below the break luminosity at any redshift, and thus will not affect our results. Likewise, this could occur at very large radius  $r \gg a$  in any  $L_{\text{peak}}$  system, but again we are not attempting to model the large-scale blastwave but only the evolution relevant to the small accretion regions.

### 2.3. Parameterizations of the Quasar Light Curve

The fits and analytical modeling above imply a useful, simple prescription for the quasar light curve as applied in semi-analytical models and other theoretical modeling which cannot resolve the detailed time history of individual objects as

we can in our simulations. Generally, the quasar light curve is characterized by two “modes”: a “growing mode,” characterized by high-Eddington ratio, rapid black hole growth, and a “decaying mode,” characterized by the nearly self-similar power-law falloff of the quasar luminosity as nearby gas is heated or expelled. The “growing mode” can be most simply parameterized by exponential growth at a constant Eddington ratio  $\dot{m}$ , with an exponential light curve  $L = L(t=0) \exp\{t/t_Q\}$ , where  $t_Q = t_S/\dot{m}$  is the  $e$ -folding time and  $t_S = 4.2 \times 10^7$  yr is the Salpeter time. Such black hole growth is expected in essentially all models of quasar activity, where plentiful fueling easily enables high accretion rates.

Once the quasar reaches a critical luminosity or mass (in e.g. accord with the  $M - \sigma$  relation), it begins to heat and expel the surrounding gas, and the accretion rate rapidly falls off – i.e. the light curve can be roughly parameterized as entering the “decay mode” described above. Our fits to the quasar lightcurves after the “blowout” phase and analytical modeling of this phase of evolution as a driven blastwave suggest a power-law decline in the quasar lightcurve, which can be simple modeled as

$$L(t)/L_{\text{peak}} \approx \dot{m} = \frac{1}{1 + (t/t_Q)^\beta}. \quad (13)$$

$L_{\text{peak}}$  here is the peak bolometric luminosity, just as the quasar enters the “blowout” phase, and  $L(t)$  is the subsequent bolometric luminosity at time  $t$  after the peak ( $L = L_{\text{peak}}$  at  $t = 0$ ). It is also not a bad approximation to use this to model both the light curve and accretion rate with  $L(t)/L_{\text{peak}} \approx \dot{m}$ , because not much total black hole mass is accumulated in this mode. The equation shown assumes  $\dot{m} \approx 1$  at peak luminosity, as is true in most of our simulations, but this can easily be renormalized to any assumed constant  $\dot{m}$  in the constant Eddington ratio “growing mode.” The functional form of this equation is chosen such that it joins continuously with the constant Eddington ratio exponential light curve at  $t = 0$  ( $L = L_{\text{peak}}$ , i.e. at the beginning of the “blowout” stage), and behaves as our fitted power-laws at times large compared to the duration of the “blowout.”

The critical behavior determined from our simulation is this power-law decay of the quasar light curve at late times,  $L(t) \propto (t/t_Q)^{-\beta}$ . We have measured  $\beta$  directly in our simulations above, and estimated its value from simple analytical models of the quasar-driven “blowout” phase. To lowest order, a canonical value of  $\beta = 2$  is suggested by both our fits to the simulation light curves and the self-similar Sedov-Taylor solution for a quasar-driven blastwave and Bondi accretion. But we have also explicitly determined  $\beta$  as a function of peak luminosity, which we inverted to determine  $\gamma(L_{\text{peak}})$  above. Our fits to the simulations yield

$$\beta \approx \beta_{12} + \frac{d\beta}{d\log L_{\text{peak}}} \{\log_{10}(L_{\text{peak}}/10^{12}L_{\odot})\}. \quad (14)$$

where  $\beta_{12} \approx 1.7 \pm 0.3$  and  $d\beta/d\log L_{\text{peak}} \approx 0.7 \pm 0.1$ . There is some ambiguity in  $\beta$  depending on whether we are fitting to a given blowout or a whole quasar lifetime which includes the “growing” phases (giving shallower effective  $\beta$ ), as can be seen directly by the fact that different values of the faint-end quasar lifetime slope  $\gamma$  are suggested by our fitting of the quasar lightcurves and our fitting of the quasar lifetime to a Schechter function. However, for most theoretical models which require a time-dependent quasar lightcurve, the parameterization desired is that of an individual blowout, and so

these fits are used to determine Equation 14 above. Furthermore, the “effective”  $\beta$  from fitting to the quasar lifetime is simply  $1/\alpha$ , which can be directly determined from the values of  $\gamma(L_{\text{peak}})$  given in Table 1. There is a significant amount of scatter around this mean relation in  $\beta$  (in contrast to the quite small scatter in  $\alpha$ ) at a given  $L_{\text{peak}}$ ,  $\Delta\beta \sim 1$ , which can easily be incorporated in theoretical models of quasar populations if desired. Clearly, this formula for  $\beta(L_{\text{peak}})$  cannot be extrapolated to arbitrary luminosities, as by definition  $\beta > 0$  always. In fact, most of the simulations which are well-fit by a very low  $\beta$  are so because they never reach a high Eddington ratio and cause a significant “blowout” event, but rather they quiescently accrete for  $\sim$ Gyr at moderate ( $\sim 0.1$ ) Eddington ratios. In either case, this is only important  $L_{\text{peak}} \lesssim$  a few  $\times 10^9 L_{\odot}$ , which implies black hole masses  $\lesssim 10^5 M_{\odot}$ , well below the regimes where the processes we have modeled should be important (and below the limits to which our simulation light curves can be reliably estimated).

There is, unfortunately, significant ambiguity in the appropriate value of  $t_Q$  to use in this simple parameterization of the quasar light curve. If we use Equation 14 to estimate the *cumulative* quasar lifetime at low luminosities ( $L \ll L_{\text{peak}}$ , low enough that the contribution from the “growing mode” is negligible) and compare this with the Schechter function fits or direct calculation of the quasar lifetime from our simulations at these luminosities, there is a well-defined approximately constant  $t_Q \approx t_S = 4.2 \times 10^7$  yr (or, if we allow  $t_Q$  to vary with  $\beta$  and demand that this match to the low-luminosity limit of the fitted Schechter function with the same  $L_{\text{peak}}$ ,  $t_Q \approx \beta t_S \sim 10^8$  yr). However, there are several minor “blowout” events in our simulations, and usually at least two major ones (one at first passage, the other after the final merger). The  $t_Q$  which we have constrained by fitting the integrated quasar lifetime is approximately the sum of these contributions. If we instead fit to  $t_Q$  in an *individual* blowout, we obtain a significantly smaller value  $t_Q \approx 10^7$  yr (as is also suggested by direct examination of Figure 1). The “appropriate” value of  $t_Q$  is then somewhat determined by the ability of a given model to resolve separate starbursts triggered by e.g. passage of galaxies as opposed to the final merger, and resolution of triggering by minor mergers. However, our simulations constrain the range of reasonable  $t_Q$  to  $\sim 10^7 - 10^8$  yr, which is still a significantly more narrow range than the observations constrain (e.g., Martini 2004). More important, to first order,  $t_Q$  only controls the normalization of various predicted quantities and it should be easily calibrated in a given theoretical model by comparison to e.g. quasar number counts and the normalization of the luminosity function. Even with these uncertainties in the proper “effective”  $t_Q$  due to the limited resolution of individual events in semi-analytical or cosmological models, the implied appropriate effective  $t_Q$  for a given model is an interesting constraint on e.g. radiative efficiencies of quasars (as the  $t_Q$  we fit scales with the  $e$ -folding time for black hole growth, and hence the radiative efficiency) and the effectiveness of quasar feedback. For example, a very short  $t_Q$ , especially in a model which is effectively summing over several different “blowout” events, implies very rapid expulsion or heating of gas and therefore highly efficient coupling of quasar energy or momentum to the surrounding gas in the “blowout” phase.

The quasar lightcurve is, of course, much more complex than we have modeled here. Not only are there several such “growing,” “blowout,” and “decaying” modes in a given

merger event, but each follows a light curve which is not trivial in detail, and our mixed exponential and power-law light curves are not always a good fit. Whenever possible, theoretical models should adopt the most accurate approximations to the quasar light curve available, attempting to resolve the detailed time history where it is important (for example, in estimating the properties and luminosity function of the faint quasar population). However, in many cases this is not possible or feasible, and a simple analytical approximation for the quasar light curve is necessary or convenient. The above simple parameterization describes both the growing and decaying phases of the quasar light curve with reasonable accuracy, and captures the critical properties of the quasar lifetime and its increase with decreasing luminosity and the tendency of bright peak luminosity quasars to spend extended periods in low-luminosity phases, and should therefore be useful in such modeling. This does not, however, include the effects of obscuration, which are not important (at least along most sightlines) in e.g. the late blowout stages, but can dramatically change the observed quasar light curve in various bands near peak luminosity, especially before the “blowout” phase (e.g., Hopkins et al. 2005b,e). These effects can be estimated from the parameterization of column density as a function of immediate and peak luminosity in Hopkins et al. (2005e), but as noted therein, these fits are only approximate and do not accurately describe the “blowout” stage in which luminosity and column density both vary rapidly.

### 3. DISCUSSION & CONCLUSIONS

Realistic, luminosity-dependent quasar lifetimes, in which quasars spend more time at lower  $L$ , imply a novel interpretation of the QLF (Hopkins et al. 2005c), in which the faint-end is composed of sources with larger  $L_{\text{peak}}$  in early growth or sub-Eddington states. The faint-end slope  $\gamma$  is then determined by the slope of the quasar lifetime vs.  $L$ , for quasars with  $L_{\text{peak}} \sim L_*$ , the break in the observed QLF corresponding directly to the *peak* in the distribution of quasar peak luminosities (BH masses) being formed at any redshift. We have determined  $\gamma$  from both a large range of hydrodynamical simulations (varying BH and host galaxy properties) and from a simple analytical model of quasar feedback and the  $M_{\text{BH}}-\sigma$  relation, and find that it is a monotonic decreasing function of  $L_{\text{peak}}$  over the range of observed  $L_*$ .

As the break luminosity  $L_*(z)$  is well-known from observations of the QLF, we use our modeling to predict  $\gamma(z)$ . Figure 3 shows our result for  $\gamma$  in the redshift interval  $z = 0 - 4$ . Above  $z \sim 2 - 3$ , the location of  $L_*$  becomes uncertain, and we consider both pure density evolution ( $L_* =$  constant or increasing, solid) and pure peak luminosity evolution (declining  $L_*$ , dashed) at higher redshifts. The yellow shaded range shows the range predicted by different fitting methods from Table 1, lines the cumulative best-fit. The form of  $L_*(z)$  is taken from Hopkins et al. (2005e,f), but is based directly on fits to the observed QLFs of Ueda et al. (2003), Richards et al. (2005), and Hasinger et al. (2005). We compare this to observations in the hard X-ray (Ueda et al. 2003, blue squares), soft X-ray (Hasinger et al. 2005, red circles), optical (cyan; Wolf et al. 2003, diamonds; Hunt et al. 2004, star; Richards et al. 2005,  $\times$ ; Pei 1995, +), and radio (green; Sadler et al. 2002, \*; Cirasuolo et al. 2005, triangle). We convert these to bolometric luminosities and re-fit or rescale  $\gamma$  with the bolometric corrections of Marconi et al. (2004), which are also discussed in detail in Hopkins et al. (2005d,e) and are similar to those in e.g. Richards et al. (2005). Although the uncertainties in the

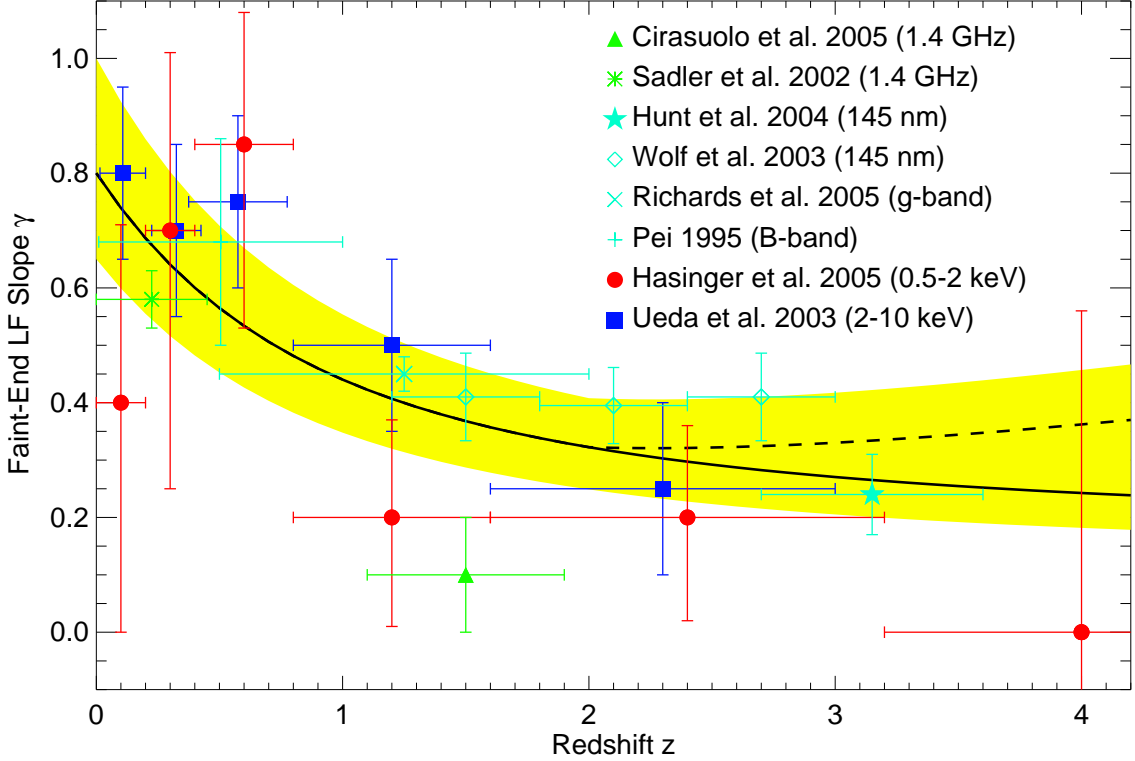


FIG. 3.— Predicted faint-end QLF slope  $\gamma$  as a function of redshift  $z$ , from the fits in Table 1. Shaded yellow shows the  $\sim 1\sigma$  range depending on fitting method, lines the mean prediction. Above  $z \sim 2$ , solid line assumes pure density evolution for the QLF, dashed line assumes pure peak luminosity evolution. Observations are shown (converted to bolometric QLF slopes) from different wavelengths as noted.

observed faint-end slope  $\gamma$  are large, we reproduce its value at all redshifts.

Figure 4 demonstrates how our prediction for the evolution of  $\gamma$  with redshift translates to a “luminosity-dependent density evolution” (LDDE). In each panel, the integrated number density  $\Phi$  (per comoving volume) of quasars in each of several luminosity intervals is plotted as a function of redshift for  $z < 5$ . The upper left shows  $\Phi$  for intervals in bolometric luminosity  $L$ :  $\log(L/L_{\odot}) = 9-10$  (black solid line),  $10-11$  (blue dotted),  $11-12$  (light blue short dashed),  $12-13$  (green dot-dash),  $12-14$  (orange triple-dot-dash), and  $14-15$  (red long dash). The effects traditionally fitted to LDDE forms are clear; the density of higher- $L$  systems rises more rapidly to a peak at higher redshift, then falls off more slowly. The difference in evolution between two  $L$  intervals becomes less dramatic with increasing  $L$ , as observed. Using the bolometric conversions of Marconi et al. (2004) described above, we also consider the observed density evolution in other bands. The upper right shows density evolution in the B-band in intervals of B-band magnitude,  $-20 > M_B > -22.5$  (black solid),  $-22.5 > M_B > -25$  (blue dotted),  $-25 > M_B > -27.5$  (green dashed),  $-27.5 > M_B > -30$  (red dot-dash). This modeling immediately demonstrates why observations in the optical have not found the dramatic LDDE seen in X-ray samples, as the effects do not become pronounced until very low luminosities not usually probed in B-band samples (as low as  $M_B \gtrsim -18$ ), and the bolometric corrections actually slightly “blur out” the effect as well. The lower left shows our prediction for the hard X-ray, in three intervals of  $L(2-10 \text{ keV}) = L_{HX}$ . In order to directly compare with the observations of

Ueda et al. (2003), we adopt cgs units and consider the intervals  $\log(L_{HX}/\text{erg s}^{-1}) = 41.5-43$  (black solid),  $43-44.5$  (blue dotted),  $44.5-46$  (green dashed). For each, we show the observed best-fit LDDE model with approximate  $1\sigma$  errors, in each observed redshift interval (filled circles of appropriate color). Likewise, the lower right shows our prediction for the soft X-ray in intervals of  $L(0.5-2 \text{ keV}) = L_{SX}$ . We compare directly to Hasinger et al. (2005) in the intervals  $\log(L_{SX}/\text{erg s}^{-1}) = 42-43$  (black solid),  $43-44$  (blue dotted),  $44-45$  (green dashed),  $45-46$  (yellow dot-dash),  $> 46$  (red triple-dot-dash). Again we show the observed best-fit LDDE model in each observed  $z$  interval (filled circles of matching color), but we have multiplied the QLF normalization of Hasinger et al. (2005) by a factor of 10 to account for the mean obscured fraction (Hopkins et al. 2005e). For all the above, we adopt pure density evolution for  $z \gtrsim 2$ . We do not show the errors in our predictions, as these are actually dominated by the uncertainty in the fitted  $n(L_{\text{peak}})$  distribution, not the uncertainty in  $\gamma(L_{\text{peak}})$ .

The results in Figure 4 show that our modeling of the quasar lifetime predicts very accurately the “luminosity-dependent density evolution” seen in X-ray samples, at all luminosities and redshifts. We may slightly underpredict the low-luminosity, high-redshift number of sources, but this is unsurprising, as it is both where the observations are most uncertain and where, for a fixed low  $L$ , the break luminosity becomes very much larger than  $L$ , meaning that our modeling is based on the quasar lifetime at  $L$  well below  $L_{\text{peak}}$  where it is most uncertain. Still, the agreement is remarkable, and it is derived almost entirely from the quasar lifetime as a function of

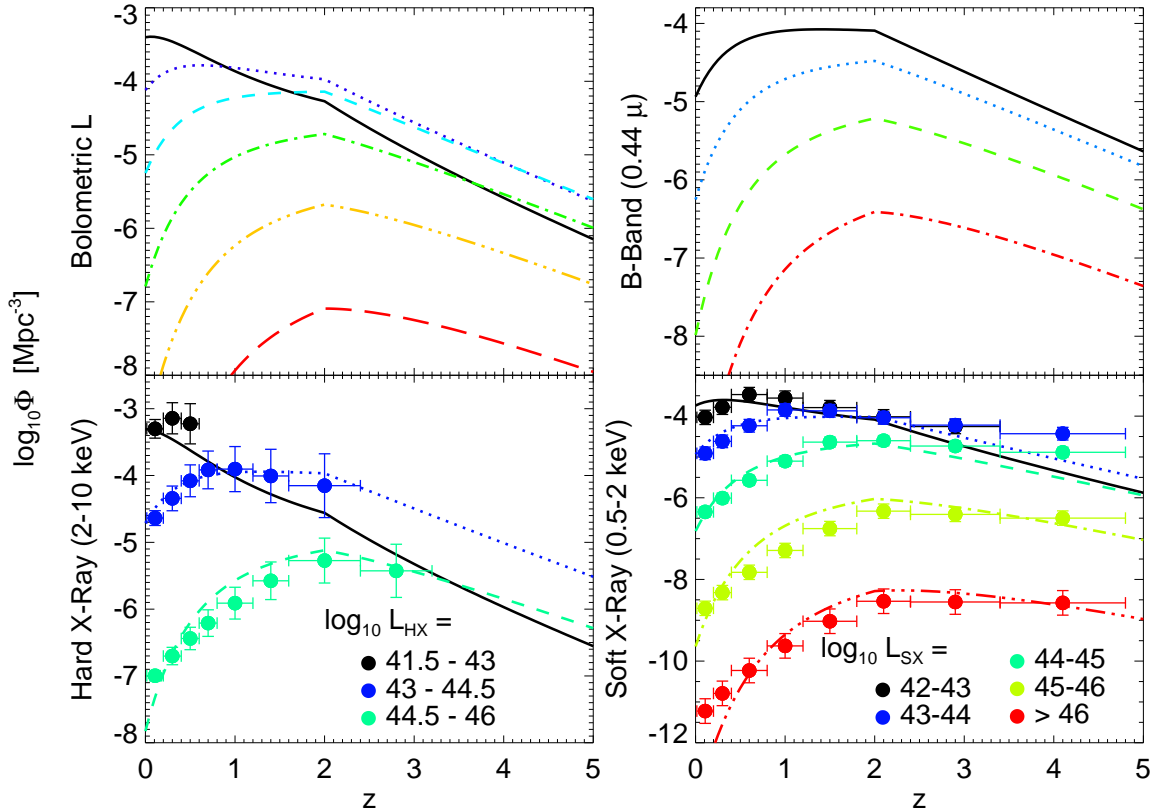


FIG. 4.— Predicted comoving number density in different luminosity intervals as a function of redshift. Upper left: Bolometric;  $\log(L/L_{\odot}) = 9-10$  (black solid line),  $10-11$  (blue dotted),  $11-12$  (light blue short dashed),  $12-13$  (green dot-dash),  $12-14$  (orange triple-dot-dash),  $14-15$  (red long dash). Upper right: B-band;  $-20 > M_B > -22.5$  (black solid),  $-22.5 > M_B > -25$  (blue dotted),  $-25 > M_B > -27.5$  (green dashed),  $-27.5 > M_B > -30$  (red dot-dash). Lower left: Hard X-ray;  $\log(L_{HX}/\text{erg s}^{-1}) = 41.5-43$  (black solid),  $43-44.5$  (blue dotted),  $44.5-46$  (green dashed), compared to observations of Ueda et al. (2003) (filled circles of corresponding color). Lower right: Soft X-ray;  $\log(L_{SX}/\text{erg s}^{-1}) = 42-43$  (black solid),  $43-44$  (blue dotted),  $44-45$  (green dashed),  $45-46$  (yellow dot-dash),  $> 46$  (red triple-dot-dash), compared to observations of Hasinger et al. (2005) (filled circles of corresponding color, normalization adjusted for obscuration).

peak luminosity. The  $n(L_{\text{peak}})$  distribution which produces the LDDE seen in Figure 4 has a simple functional form: a log-normal, with constant narrow width and normalization, and a center/peak directly related to the observed break  $L_*(z)$  in the observed QLF. In keeping with the interpretation of the QLF from Hopkins et al. (2005c), in which the faint-end is made up of brighter sources (dominated, of course, by the peak in the  $n(L_{\text{peak}})$  distribution at  $L_{\text{peak}} \sim L_*(z)$ ) in dimmer stages of their evolution, we have demonstrated that the *observed LDDE is entirely accounted for by the quasar lifetime as a function of peak luminosity, not by any change in the shape of the peak luminosity or black hole mass distribution.*

A more detailed prediction of the faint-end slope should account for several points. Sample selection effects from reddening and extinction can be significant, especially if the fraction of obscured objects is a function of luminosity (e.g., Ueda et al. 2003; Hopkins et al. 2005e). Our predictions agree best with observations from the hard X-ray, where the effect of attenuation is minimized, but a more accurate prediction of  $\gamma$  in other wavebands must account for the joint evolution of obscuration and luminosity (Hopkins et al. 2005d,e). To probe very low accretion rates  $L \ll 10^{-2}L_{\text{peak}}$ , higher-resolution simulations, with more sophisticated models for low-efficiency accretion (rates well below Bondi or Eddington) and spectral modeling of the corresponding radiatively inefficient accretion flows are needed. Further, the contribu-

tions to the faint-end QLF from quasars with  $L_{\text{peak}} \neq L_*$  (see Hopkins et al. 2005e) will introduce overall curvature into the QLF (weakening the observed break, as observed by e.g. Wolf et al. 2003; Richards et al. 2005), which may aid in constraining the  $n(L_{\text{peak}})$  distribution. Finally, at low enough  $L$  (typical of LINERs and low- $L$  Seyferts), we expect different, possibly stochastic, fueling mechanisms to contribute, which must be modeled to accurately predict the QLF shape below some limit.

Still, our simple modeling of quasar feedback, and the novel picture of the QLF resulting from the application of realistic, luminosity-dependent quasar lifetimes, accurately predicts the faint-end slope of the QLF at all observed redshifts. Our modeling provides a simple, direct physical motivation for both the break luminosity  $L_*$  and faint-end slope  $\gamma$ . The break  $L_*$  corresponds to the *peak* in the rate at which quasars with a given peak luminosity (final BH mass) are being created or activated at any given time, and  $\gamma$  is determined (to first order) by the differential lifetime of these objects, as they spend substantial time at low  $L \ll L_{\text{peak}}$ , either in early stages of rapid BH growth to larger  $L$  or in sub-Eddington states in transition into or out of the brief period of peak quasar activity. The observed  $\gamma$  and its evolution with redshift are a simple consequence of  $L_*$  and its evolution. At high- $z$ ,  $L_*$  is larger, implying most quasars have higher peak luminosity. From our simulations and analytical modeling of quasar

feedback, we expect higher- $L_{\text{peak}}$  objects to both grow and expel gas more rapidly and violently, when they reach their final mass and feedback unbinds nearby material. Thus, brighter- $L_{\text{peak}}$  objects “die” more quickly, resulting in a flatter  $\gamma$  as they spend less relative time in any given  $L < L_{\text{peak}}$ .

The observed values and evolution of  $\gamma$  provide a direct test of the model of quasar lifetimes and the QLF proposed in Hopkins et al. (2005a-f), and are not predicted by models which invoke simple “on/off” or pure exponential quasar light curves. Our model can predict  $\gamma$  as a simple function of  $L_*$ , itself tied to the characteristic quasars being created at any time, and is thus immediately useful for modeling the quasar contribution to reionization, which depends on  $\gamma$  at high- $z$ . For purposes where  $\gamma$  is important, the quasar lifetimes fitted in Hopkins et al. (2005e) should be slightly modified to be Schechter functions with faint-end slopes  $\gamma(L_{\text{peak}})$  [the weak dependence of normalization on  $L_{\text{peak}}$  found therein is entirely contained in  $\gamma(L_{\text{peak}})$ ]. We have also provided simple analytical forms for the quasar light curve, for use in semi-analytical models and other theoretical models of which require the time-dependent quasar light curve (not simply the statistical properties contained in the quasar lifetime fits we have previously calculated), and which cannot resolve the detailed time dependence of quasar activity in individual mergers and interactions. We have demonstrated that the observed evolution of  $\gamma$  and corresponding “luminosity-dependent density evolution” of the quasar population are not just accounted for, but actually *predicted* in our model of the QLF, as a consequence of quasar feedback being more violent in higher peak luminosity (larger BH mass) systems, and the fact that the observed faint-end QLF is dominated by sources with intrinsically brighter peak luminosity ( $L_{\text{peak}} \sim L_*(z)$ ) in dimmer stages of their evolution.

While more accurate predictions require additional detailed modeling, the results presented here allow future observations of  $\gamma$  to directly constrain the differential quasar lifetime, even at  $L \ll L_{\text{peak}}$ , as our modeling shows that the faint-end QLF effectively traces the quasar *lifetime* of  $L_{\text{peak}} \sim L_*$  sources, *not* the intrinsic source (e.g. peak  $L$  or BH mass) distribution. Such observations will further limit models of the distribution of quasar masses and host properties [through  $n(L_{\text{peak}})$ ], and models of quasar fueling mechanisms and accretion (through the form of the lifetime/slope at low- $L$ ). As is clear in Figure 3, the QLF faint-end slope as a function of redshift is still only poorly constrained by observations. Improved observational constraints, in particular samples with a uniform selection criteria which can span the range of redshifts  $z = 0 - 6$ , for which the selection criteria could be accurately modeled and compared in detail with observations, would provide very valuable constraints on theoretical models of quasar feedback, e.g. determining the relative contributions to the faint-end QLF from quasars growing to larger luminosities or relaxing after their peak, and constraining the efficiency of coupling between accretion energy and the surrounding ISM. Samples which cover the relevant redshift range in a uniform rest frame wavelength are also especially valuable, and measurements in different wavelengths can provide different constraints. For example, the faint-end hard X-ray QLF may be more robust against obscuration effects and so provide a better indicator of the bolometric luminosity function, tracing e.g. relatively low-luminosity stages hidden by circumnuclear starbursts. The optical QLF, on the other hand, is in our modeling more closely associated with the peak quasar luminosity and “blowout” phase, meaning that the faint-end optical QLF (measurement

of which would require extending the completeness of current high-redshift optical surveys by several magnitudes) can provide an valuable constraint on the underlying peak luminosity distribution, a particularly valuable quantity in itself because it determines, in our modeling, the QLF in all other bands, and reflects (as well as constrains) much more directly the underlying cosmological context, such as merger rates as a function of host galaxy mass. The combination of the two, yielding a reliable bolometric faint-end luminosity function slope and underlying peak luminosity distribution, would allow measurements of  $\gamma(z)$  to be translated reliably into  $\gamma(L_{\text{peak}})$ , and could be de-convolved to construct an entirely observational determination of the quasar lifetime as a function of luminosity. These observations, though difficult at very high  $z$ , can probe redshifts at which direct observations of quasar hosts and masses are inaccessible, constraining theories of early quasar evolution.

Combined with the modeling presented in Hopkins et al. (2005a-f), this motivates a completely self-consistent picture of the quasar lifetime and luminosity function, derived from the input physics of our simulations and without arbitrary tunable parameters. With the critical recognition that the quasar lifetime is *luminosity-dependent*, with quasars spending more time at low luminosities than their peak luminosities (as has now also been suggested by observations, e.g. Adelberger & Steidel 2005), we have shown that a large range of observed properties of the quasar and spheroid population are predicted to high accuracy, over a wide range of observed redshifts. These works also provide several simple tests of our model of the quasar lifetime, and correspondingly the model of the faint-end slope presented here. In Hopkins et al. (2005a-e), we explicitly demonstrate that these predictions include, e.g. the QLF at frequencies from optical to hard X-ray and at many observed redshifts, the distribution of Eddington ratios as a function of luminosity and redshift, the column density distribution at various wavelengths, the fraction of broad-line quasars as a function of luminosity and redshift, the active BH mass function of both Type I and Type II quasars, the relic BH mass function and total density, the cosmic X-ray background spectrum, the anti-hierarchical evolution of BH mass, the radio source population at high redshift, correlations between IR emission, star formation, and quasar obscuration, and the quasar lifetime as a function of luminosity and host galaxy properties. The distribution of Eddington ratios as a function of luminosity is a direct test of this model, and the degree to which typical Eddington ratios decrease below the break in the observed luminosity function informs the extent to which the faint-end slope is dominated by sources at  $L_{\text{peak}} \sim L_*$ . Likewise, the active BH mass function constrains the  $n(L_{\text{peak}})$  distribution, and an accurate measurement of its peak can be used to determine the  $L_{\text{peak}}$  which dominates the faint-end slope, providing a direct means to constrain the slope  $\gamma$  as a function of  $L_{\text{peak}}$ . The broad line fraction as a function of luminosity can provide a similar constraint, as the luminosity at which the QLF transitions to being broad-line dominated is of order the turnover luminosity in the Schechter function fit to the quasar lifetime for  $L_{\text{peak}} \sim$  the peak of the  $n(L_{\text{peak}})$  distribution.

Further, Lidz et al. (2005) show this model also predicts the correlation function and bias of quasars as a function of luminosity and redshift, and the quasar-galaxy cross-correlation function, dramatically different from the prediction in models with a simple quasar lifetime. The mean quasar bias (noting that the bias depends on luminosity much more weakly in

our model than in simpler models of the quasar lifetime) is a direct probe of typical quasar host halo masses, constraining the peak in the  $\dot{n}(L_{\text{peak}})$  distribution and thus allowing for a determination of  $\gamma(L_{\text{peak}})$ . The steepness of the bias vs. luminosity is sensitive to the width of the  $\dot{n}(L_{\text{peak}})$  distribution, and thus limits the contribution of quasars with  $L_{\text{peak}} \neq L_*$  to the faint-end slope. Thus far the observations (e.g. Croom et al. 2005, Adelberger & Steidel 2005) support a picture of a peaked  $\dot{n}(L_{\text{peak}})$  distribution in close agreement with our modeling, but the bias as a function of luminosity is still only poorly determined by observations.

Hopkins et al. (2005f) extend these predictions to the properties of spheroids and red galaxies, self-consistently and accurately predicting (from the observed *quasar* luminosity function) the distribution of velocity dispersions, the mass function, mass density, and star formation rates, the luminosity function in a wide range of observed wavebands, the total red galaxy number density and luminosity density, the distribution of colors as a function of magnitude and velocity dispersion for various color-magnitude combinations, and the distribution of formation redshifts/ages as a function of both mass and luminosity, each as a function of redshift at different observed redshifts. Our modeling also reproduces the X-ray emitting gas properties (Cox et al. 2005), morphologies and metallicities (Cox et al. 2005, in preparation),  $M_{\text{BH}} - \sigma$  relation (Di Matteo et al. 2005) and fundamental plane relation (Robertson et al. 2005, in preparation), the dispersion about each relation (Robertson et al. 2005), and bimodal color distribution (Springel et al. 2005a) of observed galaxies. The distribution of these properties and e.g. spheroid luminosity and mass functions can be used to constrain the form of the quasar lifetime based on purely observational arguments, by using observed correlations between e.g. stellar or virial mass and BH mass in the context of the merger hypothesis of elliptical galaxy formation to determine the underlying rate at which

galaxies of a given final (combined) stellar mass must merge to produce the remnant spheroid population and its evolution with redshift (essentially determining the differential growth with time and mass) and from this the corresponding  $\dot{n}(L_{\text{peak}})$  distribution. Having determined the rate at which quasars of a given peak luminosity are created, a de-convolution of the observed quasar luminosity function and  $\dot{n}(L_{\text{peak}})$  can constrain the allowed range of quasar lifetimes as a function of peak luminosity (essentially the reverse of our modeling, in which we de-convolve the QLF and quasar lifetime to determine  $\dot{n}(L_{\text{peak}})$ ).

The wide range of observations predicted by this model provides a number of very different means by which to observationally test both the qualitative picture proposed and the detailed dependence of quasar lifetime and corresponding faint-end QLF slope on quasar peak luminosity. We have demonstrated that a proper modeling of quasar evolution, including the critical effects of quasar feedback on the host galaxy in major mergers, can completely account for (and in fact *predicts*) the detailed evolution of the faint-end QLF slope and luminosity-dependent density evolution, without fitting to the faint-end observations or fine-tuning any parameters, and is entirely self-consistent with the large number of detailed observations above, as a simple consequence of realistic, physically motivated, *luminosity-dependent* quasar lifetimes.

This work was supported in part by NSF grants ACI 96-19019, AST 00-71019, AST 02-06299, and AST 03-07690, and NASA ATP grants NAG5-12140, NAG5-13292, and NAG5-13381. The simulations were performed at the Center for Parallel Astrophysical Computing at the Harvard-Smithsonian Center for Astrophysics.

#### REFERENCES

- Adelberger, K. L. & Steidel, C. C. 2005, ApJ, in press [astro-ph/0505210]  
 Barkana, R., & Loeb, A. 2001, Phys. Rep., 349, 125  
 Barnes, J.E. & Hernquist, L. 1991, ApJ, 370, L65  
 Barnes, J.E. & Hernquist, L. 1996, ApJ, 471, 115  
 Bondi, H. 1952, MNRAS, 112, 195  
 Bondi, H. & Hoyle, F. 1944, MNRAS, 104, 273  
 Bullock, J. S., Dekel, A., Kolatt, T. S., Kravtsov, A. V., Klypin, A. A., Porciani, C., & Primack, J. R. 2001, ApJ, 555, 240  
 Ciotti, L. & Ostriker, J. P. 2001, ApJ, 551, 131  
 Cirasuolo, M., Magliocchetti, M., & Celotti, A. 2005, MNRAS, 357, 1267  
 Cowie, L. L., Barger, A. J., Bautz, M. W., Brandt, W. N., & Garmire, G. P. 2003, ApJ, 584, L57  
 Cox, T. J., Di Matteo, T., Hernquist, L., Hopkins, P. F., Robertson, B., & Springel, V. 2005, ApJ, submitted [astro-ph/0504156]  
 Croom, S. M., et al. 2005, MNRAS, 356, 415  
 Di Matteo, T., Springel, V., & Hernquist, L. 2005, Nature, 433, 604  
 Fabian, A. C. 1999, MNRAS, 308, L39  
 Fiore, F., et al. 2003, A&A, 409, 79  
 Furlanetto, S. R., & Loeb, A. 2001, ApJ, 556, 619  
 Hasinger, G., Miyaji, T., & Schmidt, M. 2005, A&A, in press [astro-ph/0506118]  
 Hernquist, L. 1990, ApJ, 356, 359  
 Hopkins, P. F., Hernquist, L., Martini, P., Cox, T. J., Robertson, B., Di Matteo, T., & Springel, V. 2005a, ApJ, 625, L71  
 Hopkins, P. F., Hernquist, L., Cox, T. J., Robertson, B., Di Matteo, T., Martini, P., & Springel, V. 2005b, ApJ, accepted [astro-ph/0504190]  
 Hopkins, P. F., Hernquist, L., Cox, T. J., Robertson, B., Di Matteo, T., & Springel, V. 2005c, ApJ, accepted [astro-ph/0504252]  
 Hopkins, P. F., Hernquist, L., Cox, T. J., Robertson, B., Di Matteo, T., & Springel, V. 2005d, ApJ, accepted [astro-ph/0504253]  
 Hopkins, P. F., Hernquist, L., Cox, T. J., Robertson, B., Di Matteo, T., & Springel, V. 2005e, ApJ, submitted [astro-ph/0506398]  
 Hopkins, P. F., Hernquist, L., Cox, T. J., Robertson, B., Di Matteo, T., & Springel, V. 2005f, ApJ, submitted [astro-ph/0508167]  
 Hunt, M. P., Steidel, C. C., Adelberger, K. L., & Shapley, A. E. 2004, ApJ, 605, 625  
 Kauffmann, G. & Haehnelt, M. 2000, MNRAS, 311, 576  
 La Franca, F., et al. 2002, ApJ, 570, 100  
 Lidz, A., Hopkins, P. F., Cox, T. J., Hernquist, L., Robertson, B., Di Matteo, T., & Springel, V. 2005, ApJ, submitted [astro-ph/0507361]  
 Mac Low, M., & Ferrara, A. 1999, ApJ, 513, 142  
 Marconi, A., & Hunt, L.K. 2003, ApJ, 589, L21  
 Marconi, A., Risaliti, G., Gilli, R., Hunt, L. K., Maiolino, R., & Salvati, M. 2004, MNRAS, 351, 169  
 Martini, P. 2004, in Carnegie Obs. Astrophys. Ser. 1, Coevolution of Black Holes and Galaxies, ed. L.C. Ho (Cambridge: Cambridge Univ. Press), 170  
 Merloni, A. 2004, MNRAS, 353, 1035  
 Mihos, J.C. & Hernquist, L. 1996, ApJ, 464, 641  
 Miyaji, T., Hasinger, G., & Schmidt, M. 2000, A&A, 353, 25  
 Miyaji, T., Hasinger, G., & Schmidt, M. 2001, A&A, 369, 49  
 Murray, N., Quataert, E., & Thompson, T. A. 2005, ApJ, 618, 569  
 Narayan, R. & Yi, I. 1995, ApJ, 452, 710  
 Ostriker, J. P., & McKee, C. F. 1988, Reviews of Modern Physics, 60, 1  
 Page, M. J., Mason, K. O., McHardy, I. M., Jones, L. R., & Carrera, F. J. 1997, MNRAS, 291, 324  
 Pei, Y. C. 1995, ApJ, 438, 623  
 Richards, G. T. et al. 2005, in press [astro-ph/0504300]  
 Robertson, B., Yoshida, N., Springel, V., & Hernquist, L. 2004, ApJ, 606, 32  
 Robertson, B., Hernquist, L., Cox, T. J., Di Matteo, T., Hopkins, P. F., Martini, P., & Springel, V. 2005, ApJ, submitted [astro-ph/0506038]  
 Sadler, E. M., et al. 2002, MNRAS, 329, 227  
 Scannapieco, E., & Oh, S. P. 2004, ApJ, 608, 62  
 Sedov, L. I. 1946, Prikl. Mat. Mekh. 10, 241, No. 2  
 Sedov, L. I. 1959, Similarity and Dimensional Methods in Mechanics, New York: Academic Press, 1959

- Silk, J. & Rees, M. J. 1998, A&A, 331, L1  
Springel, V. 2005, MNRAS, submitted, [astro-ph/0505010]  
Springel, V., Di Matteo, T., & Hernquist, L. 2005a, ApJ, 620, L79  
Springel, V., Di Matteo, T., & Hernquist, L. 2005b, MNRAS, 361, 776  
Springel, V. & Hernquist, L. 2002, MNRAS, 333, 649  
Springel, V. & Hernquist, L. 2003, MNRAS, 339, 289  
Springel, V. & Hernquist, L. 2005, ApJ, in press [astro-ph/0411379]  
Taylor, G. I. 1950, Proc. R. Soc. London, Ser. A 201, 175  
Ueda, Y., Akiyama, M., Ohta, K., & Miyaji, T. 2003, ApJ, 598, 886  
Wolf, C., Wisotzki, L., Borch, A., Dye, S., Kleinheinrich, M., & Meisenheimer, K. 2003, A&A, 408, 499  
Wyithe, J. S. B. & Loeb, A. 2002, ApJ, 581, 886  
Wyithe, J. S. B. & Loeb, A. 2003, ApJ, 595, 614